NON-CONICAL SEPARATED FLOW ABOUT SLENDER BODIES AT INCIDENCE

ICAS-94-5.7.2

Ann L. Gaitonde*
S.P. Fiddes
Department of Aerospace Engineering
University of Bristol
Bristol, United Kingdom

Abstract

An inviscid vortex-sheet model for non-conical separated flows about slender bodies at incidence and yaw to a uniform stream is described. The vortex-sheet model has previously been used to model conical flows past thin conical wings and smooth slender conical bodies. Modelling of non-conical flows using the simpler line-vortex model has been described for thin wings and smooth slender bodies, where each of the separated shear layers is represented by a line-vortex, joined to a specified separation line by a cut. However, previous to this study, the vortex-sheet model had only been implemented for thin wings. The cross-sections of the bodies considered here are either circular or basically square or triangular, but with rounded corners. Studies of cones with these cross-sections and of elliptic cones has revealed that cross-sectional shape has a strong influence on the degree of asymmetry. Since the model is inviscid and there are no salient edges to fix separation, separation lines must be specified *a priori*. Results are presented for both symmetric and asymmetric non-conical flows past smooth slender bodies.

1 INTRODUCTION

When a slender body is placed in a flow at moderate to high incidence boundary layers develop on either side of the windward attachment line and eventually separate to form free shear layers that roll up into concentrated vortex cores running from the apex along the length of the body. Flows of this type occur on aircraft and missile forebodies and can develop large forces which are important when considering stability and control of the vehicle. Most strikingly, the asymmetrical development of vortices on symmetric bodies being flown without yaw can produce large side forces, which may exceed the available control power of the vehicle. The mechanism which leads to this "phantom yaw" has long been the subject of debate. It is not possible to discern from experiments whether this phenomenom is viscous or inviscid in origin. Therefore theoretical models for this problem have been developed. If high Reynolds numbers flows are considered, then the shear layers are thin and may be regarded as vortex sheets of infinite extent. The inviscid vortex-sheet model, originally described by Legendre [1] and implemented by Smith [2] has been used in this work. In this model only a finite part of the vortex sheet is represented and the remainder of the sheet including the infinite spiral of the core is represented by a line vortex joined to the free end of the sheet by a cut, see figure 1. This model has been used extensively to model conical separated flow past thin conical wings and slender conical bodies, see Fiddes [3]. Conical flow is a similarity solution of the general non-conical model, which reduces the number of variables on which the flow depends from three to two. The solution need only be constructed in one cross-flow plane, the flow field in any other cross-flow plane is then found by a linear scaling of this solution. Non-conical flows have been modelled for both wings (see Smith [4]) and smooth slender bodies (see Fiddes [5]) using a simpler line-vortex model, however the vortex-sheet model has only previously been applied to wings (see Clark [6]). The extension of the vortex-sheet model to non-conical separated flows past smooth slender bodies is described in this paper. For non-conical flows, the solution procedure consists of a downstream-marching scheme starting from an known solution at the nose. In general a starting solution is not available, however if each body and flow considered is assumed conical at the nose then conical solutions, found previously, can be used to start the calculation procedure. Two different families of solutions have been identified on slender conical bodies of circular, elliptic, "square" and "triangular" cross-section. For laterally symmetric configurations with symmetric separation positions and no yaw, the first family solutions are symmetric, whereas the second family solutions are asymmetric. Both first and second family solutions are used as starting solutions for the downstream marching procedure.

*Formerly Ann L. Williams

2 SOLUTION PROCEDURE

Let $Oxyz$ be a rectangular Cartesian coordinate system. The origin O is at the apex of the body, Ox is directed downstream along the body's longitudinal axis, Oy is to starboard and Oz is upwards, see figure 1. Let U be the speed of the free stream at small incidence angle α and yaw angle β to the body. The velocity potential Φ of the flow can be constructed as the sum of two terms,

$$\Phi = Ux + \phi \tag{1}$$

where ϕ is the perturbation potential including incidence and yaw. For a slender body $\phi = O(k^2)$ provided incidence, α, and yaw, β are $O(k)$, where k is a small slenderness parameter, see Ashley and Landahl [7]. The solution for ϕ is a singular perturbation problem. In an inner region close to the body slenderness scalings are appropriate, that is the cross-flow coordinates y and z are small compared to x, the longitudinal coordinate along the body axis. In fact y and z are $O(kx)$. In this inner region the governing equation for the perturbation potential to leading order is a two-dimensional Laplace equation

$$\frac{\partial^2\phi}{\partial y^2} + \frac{\partial^2\phi}{\partial z^2} = 0 \tag{2}$$

provided $\left|1 - M_\infty^2\right| = O(1)$. This study concentrates on this inner region, the outer region would only be required if absolute pressures were to be determined. This would require matching of the outer limit of the inner solution to the inner limit of the outer solution. The following boundary conditions must be applied. Firstly the solution must match to the outer flow as $(y^2+z^2) \to \infty$ and the flow must be tangential to the three-dimensional body surface, the latter condition means that the body cross-section is not a streamline of the two-dimensional cross-flow. The vortex sheets are free boundaries of the potential flow region and so boundary conditions must be imposed on them. Following Smith [8], the condition that the vortex sheets must sustain no pressure jump is

$$U\frac{\partial\Delta\phi}{\partial x} = -\frac{\partial\Delta\phi}{\partial\sigma_1}\mathrm{cosec}(\varphi_1)\left\{\frac{\partial\phi}{\partial n_1}\cos(\varphi_1) + \left.\frac{\partial\phi}{\partial\sigma_1}\right|_m \sin(\varphi_1)\right\} \tag{3}$$

and the second condition that the vortex sheets are stream surfaces of the three-dimensional flow is

$$\frac{\partial\phi}{\partial n_1} = -U\frac{\partial r_1}{\partial x}\sin(\varphi_1) \tag{4}$$

The subscript 1 is used to indicate quantities in the physical cross-flow plane. In (3) and (4), Δ denotes the difference operator across the sheet, which when moving along the sheet in the direction of increasing σ_1 is defined to be 'r.h.s. - l.h.s.', r is the radius and φ_1 is the angle between the sheet and the radius vector in the cross-flow plane, see figure 1. Also $(\partial\phi/\partial\sigma_1)_m$ is the mean of the tangential velocities on either side of the sheet and $\partial\phi/\partial n_1$ is the normal velocity to the sheet in the cross-flow plane.

A condition analogous to the Kutta condition is applied at the base of each sheet. The sheet leaves the body tangentially at the separation line. On the upstream side of the separation line the velocity vector merely has to be parallel to the common tangent plane of the sheet and body. On the downstream side of the sheet, the flow must be that appropriate to flow in a cusped region, so the velocity at the base of the sheet must be tangential to the separation line. Therefore on the downstream side of the sheet the tangential velocity, V_{t1} is

$$\frac{V_{t1}}{U} = \frac{dz_{1s}}{dx}\sin\psi_1 + \frac{dy_{1s}}{dx}\cos\psi_1 \tag{5}$$

where y_{1s} and z_{1s} are the cross-flow coordinates of the separation position and ψ_1 is shown in figure 1.

The inner part of the vortex core is represented by an isolated vortex and cut, and the final condition is that the force on the vortex and cut must vanish. This is most easily expressed in terms of a complex potential $W(Z_1) = \phi + i\Psi_1$, where $Z_1 = y_1 + iz_1$, then

$$\overline{\frac{\Gamma}{U}\lim_{Z_1\to Z_{1V}}\left\{\frac{dW}{dZ_1} - \frac{\Gamma}{2\pi i}\right\}} = \overline{\left[(Z_{1V} - Z_{1E})\frac{d\Gamma}{dx} + \Gamma\frac{dZ_{1V}}{dx}\right]} \tag{6}$$

where the positions of the isolated vortex and the "free end" of the finite part of the sheet in the Z_1 (or physical) plane, are given by Z_{1V} and Z_{1E} respectively, and Γ is the circulation of the isolated vortex, see Clark [6].

The construction of the complex potential W, or the complex conjugate velocity dW/dZ_1 is complicated in the physical plane and thus for simplicity the region outside the body cross-section, with cross-sectional reference length $h(x)$, is mapped to the region exterior to a circle, radius $l(x)$. The mapping between a rounded corner polygon and a circle is described by Williams [9], the shape of the "polygon" is a function of two mapping parameters λ and μ. In the circle, or Z_2, plane the complex conjugate velocity is more easily constructed using the linearity of the governing equations and the method of images. For simplicity, non-dimensional variables are introduced, velocities are scaled by U, the free stream velocity and cross-sectional lengths by $l(x)$ the radius of the transformed circle. The complete separated flow complex conjugate velocity is therefore written in terms of non-dimensional variables as

$$(v_1 - iw_1) = \frac{dW}{dZ_1}$$

$$= \frac{dZ_2}{dZ_1}\left\{(\beta - i\alpha) - \frac{\beta + i\alpha}{Z_2^2} + \sum_{n=0}^{\infty}\frac{(\tilde{A}_n + i\tilde{B}_n)}{Z_2^{n+1}}\right.$$

$$+\frac{1}{2\pi i}\sum_{j=1}^{2}\left(\Gamma_j\left[\frac{1}{Z_2-Z_{2V}(j)}-\frac{1}{Z_2-\frac{1}{\overline{Z}_{2V}(j)}}\right]+\right.$$

$$\left.\int_0^{\sigma_{jmax}}\frac{\partial\Delta\phi}{\partial\sigma_2}\left[\frac{1}{Z_2-Z_{2V}(j)}-\frac{1}{Z_2-\frac{1}{\overline{Z}_{2V}(j)}}\right]d\sigma_2\right)\Bigg\} \tag{7}$$

where $\tilde{A}_n$ and $\tilde{B}_n$ are Fourier coefficients used in the series representation of the the component of the normal velocity to the body in the cross-flow plane and in (7) give the attached flow component at zero incidence and yaw. For a body of fixed cross-section once $\tilde{A}_n$ and $\tilde{B}_n$ are known in one cross-flow plane, they can be found in any other cross-flow plane by scaling. However where the cross-sectional shape varies, $\tilde{A}_n$ and $\tilde{B}_n$ must be recalculated in each plane where the velocity is required, see Williams [10]. The integrals in (7), which represent the contribution of the vortex sheets to the velocity cannot be evaluated analytically, nor using simple numerical integration schemes (eg Simpson's rule) which have unbounded errors. Instead a panel method is adopted, however this cannot take place in the Z_2 (circle) plane since the curvature at the base of the sheet may be infinite. Thus a series of mappings is carried out for each sheet, see figure 2, so that in the final Z_{5j} plane the curvature of the jth sheet is everywhere finite. The jth sheet may then be represented as a series of circular arc panels in this Z_{5j} plane, with continuous tangent angle and sheet strength along the sheet. The values of strengths and sheet tangent angles at panel end points in the Z_{5j} plane, together with the circulation and position in the Z_2 plane of each of the isolated vortices, representing the cores, give $2(n_1+n_2+3)$ unknowns to be found in each cross-flow plane. The unknowns are determined from the implementation of the boundary conditions (note that the sheet tangent angle at the base of the jth sheet is fixed by the condition that the sheet leaves the body tangentially and has strength zero in the Z_{5j} plane and are therefore known). The method by which the vortex sheet contribution to the complex conjugate velocity is calculated in this Z_{5j} plane follows exactly the method for conical flow. This process is explained in detail by Williams [10] and is not repeated here.

The vector of unknowns in each cross-flow plane are represented by $\underline{Y}(x)$. If the solution $\underline{Y}_i$ in the plane $x=x_i$ is known, then a marching procedure is used to advance the solution to the plane $x=x_{i+1}$, where $x_{i+1}=x_i+h_i$ and h_i is the ith step length in the downstream direction. The stream surface and pressure conditions (3) and (4) must be satisfied at internal panel end points and at the midpoint of the panel at the free end of the sheets, together with the force conditions (6) and the Kutta conditions (5), in a plane $x=x_{i+p}$, where $x_{i+p}=x_i+ph_i$ and $0\le p\le 1$ using a finite difference procedure to estimate derivatives. Streamwise derivatives of flow quantities are then approximated using

$$\left.\frac{df}{dx}\right|_{i+p}=\frac{f_{i+1}-f_i}{x_{i+1}-x_i} \tag{8}$$

and all dimensional quantities other than streamwise derivatives are evaluated at $x=x_{i+p}$ using linear interpolation.

$$f_{i+p}=pf_{i+1}+(1-p)f_i \tag{9}$$

The following values of the finite difference parameter p are special cases

$p=0$ Forward difference scheme, Explicit Euler.
$p=1$ Backward difference scheme, Implicit Euler.
$p=0.5$ Central difference scheme.

A similar central difference scheme was adopted by Jones [11] for rolling wing and body combinations.

The boundary conditions can now be applied using the finite differences given above to estimate derivatives and linear interpolation to estimate the solution in the plane $x=x_{i+p}$. This estimate to the solution at $x=x_{i+p}$ can be used to evaluate all the quantities required in the boundary conditions which give $2(n_1+n_2+3)$ equations for the $2(n_1+n_2+3)$ unknowns. The Kutta conditions (5), applied at the base of each sheet, can be solved simultaneously to determine Γ_1 and Γ_2 in the plane $x=x_{i+1}$ in terms of the position and strength of the vortex sheets and the position of the cores in the $x=x_i$ and the $x=x_{i+1}$ planes. These expressions can be introduced into the remaining $2(n_1+n_2+2)$ non-linear equations, reducing the number of unknowns to be solved for by two. These equations are solved using a multi-dimensional Newton-Raphson scheme similar to that used by Barsby [12].

Initial attempts to generate solutions of the problem were carried out with $p=0.5$, since a central difference scheme is accurate to second order in h_i. For some body shapes and angles of incidence, the development of the solution from an initial conical form could be calculated with no apparent difficulty for a considerable distance downstream. In other cases, instabilities are encountered which lead to a failure of the Newton method to converge, often after only a few steps. Central difference schemes are prone to instabilities and some solutions generated by this method showed fluctuations in the sheet shape in successive planes. At this stage it was not clear if the "waves" were a result of the numerical method or a genuine feature of the solution. Investigations of the effect of step size h_i, the value of p and tolerance were therefore carried out. It was found that decreasing p below 0.5 made progress downstream impossible for all the cases considered. Therefore the only values of p considered are $0.5\le p\le 1$. It was found that increasing p removed the problem of fluctuations, however if p was too large for a particular problem then, again, it was not possible to move downstream.

Some of these points are illustrated in figure 3. The solutions are for a first family solution with slightly asymmetric separation positions specified at the nose, which are made symmetric downstream on a circular cone, for various values of step size and p. Figure 3a and 3b demonstrate the effect of the choice of p. Figure 3a shows the solution with step size equal to 0.5 and $p = 0.5$. Instabilities are encountered only a short distance downstream, however increasing p to 1 and keeping the step size fixed overcomes this problem, shown in figure 3b. Figures 3b and 3c show the effect of step size at fixed $p = 1$. Figure 3b has step size 0.5, whilst figure 3c shows the solution when the step size is halved to 0.25. Clearly the solutions are unaffected by this change.

3 RESULTS

Two programs were written; one where lateral symmetry was enforced and one where asymmetry was permitted.

For the non-conical problems considered in this paper the body cross-sectional reference length, $h(x)$, is assumed to have one of the three longitudinal distributions:

TYPE 1 The body cross-sectional reference length follows a cone. The non-conical calculation arises by virtue of a longitudinal variation of the separation positions or body shape parameter. The body reference length is given by

$$h(x) = x \tan \nu^o \tag{10}$$

TYPE 2 Body varies smoothly from one cone via a circular arc to another cone of small apex angle. The cross-sectional reference length is given by

$$\begin{array}{rcll} h(x) & = & x \tan \nu_1^o & 0 < x < a \\ R^2 & = & (h(x) - f)^2 + (x - g)^2 & a < x < b \\ h(x) & = & h(b) + (x - b) \tan \nu_2^o & b < x \end{array} \tag{11}$$

where a, b, ν_1 and ν_2 are specified and f, g, R and $h(b)$ are calculated to make h and dh/dx continuous functions of x. A sketch of a typical body is shown in figure 4a.

TYPE 3 Body varies smoothly from a cone via a circular arc to a cylindrical afterbody. The cross-sectional reference length is given by

$$\begin{array}{rcll} h(x) & = & x \tan \nu_1^o & 0 < x < a \\ R^2 & + & (h(x) - f)^2 + (x - g)^2 & a < x < b \\ h(x) & = & h(b) & b < x \end{array} \tag{12}$$

where a, b, and ν_1 are specified and f, g, R and $h(b)$ are calculated to make h, dh/dx continuous functions of x. A sketch of a typical body is shown in figure 4b.

3.1 SYMMETRIC SOLUTIONS

First, consider a body of TYPE 2, where $\nu_1 = 5^o, \nu_2 = 3^o, a = 5.0$ and $b = 12.0$. Figure 5 shows the vortex-sheet shapes in successive cross-flow planes for a body of "square" cross-section placed side onto the incident flow where $\mu = 0.8, \lambda = 0.5, \theta_{2s}(1) = 38.96^o$ and $\alpha = 3.0 \tan 5^o$. The solution furthest downstream is at $x = 40.6$. It is clear that the solution on the conical afterbody has converged to the conical solution corresponding to the higher relative incidence there. This is also shown by the longitudinal variation of the normal force coefficient and the non-dimensional total circulation, shown in figure 6. This geometric test case helped to validate the method, since no experimental or theoretical results were available for comparison.

Next, consider bodies of TYPE 3 with a = 3.0, b =23.0 and $\nu_1 = 5^o$. These bodies are conical at the nose and move smoothly to cylindrical afterbodies, with a fixed cross-sectional shape for all values of x.

The vortex sheet solution proceeds downstream with an integration step of size 0.4 and $p = 0.5$. The solution for a body of circular cross-section is shown in figure 7. A downstream convergence of the cross flow plane coordinates of the line vortices representing the cores, was observed. The rate of change of the magnitude of the total circulation of the feeding sheet and core, shown in figure 8, decreases towards zero as x increases. Note that this curve is noisy due to the use of finite differences. This suggests that either for sufficiently large, but finite, x, the feeding sheet strength reaches zero and the vortices representing the cores may be stationary on the leeward side of the body with constant circulation or the feeding sheet strength asymptotes to zero, then the vortices tend to a fixed position as $x \to \infty$. This behaviour is similar to that found by Föppl for the two-dimensional case of an infinite cylinder moving through a fluid with constant velocity perpendicular to its axis, followed by a vortex pair symmetrically situated with respect to the line of advance of the centre. He found a curve on which the vortices could maintain their position relative to the cylinder provided they had a particular circulation depending on their position on the curve, see Lamb [13].

It was therefore decided to make a comparison between the appropriate Föppl curves and the vortex sheet solution on the cylindrical section. It would appear that the cores do converge onto the Föppl curve, as in figure 7. This is shown more clearly in figure 9, where the positions of the line vortices on the cylindrical section are plotted for the right hand sheet, where it appears that the vortex cores converge to a point on the the Föppl curve. If the total circulation in each cross-flow plane is used to calculate the corresponding points on the Föppl curve then these points overshoot the point to which the cores are converging. The position of the centroid of circulation in succes-

sive cross-flow planes was also calculated, see figure 9, it is possible that further downstream the centroids may converge onto the Föppl curve at a point closer to that predicted on the basis of the total circulation. Figure 10 shows the symmetrical vortex development for a body of "square" cross-section placed side onto the incident stream, $\mu = 0.8, \lambda = 0.5, \theta_{2s}(1) = 38.96^o$ and $\alpha = 3.0 \tan 5^o$. The solution furthest downstream is at $x = 37.0$. A similar convergence of the isolated vortices on the cylindrical section is observed. This suggests the existence of stationary vortex positions behind a "square cylinder" with side on to the flow, similar to the Föppl curve. A Föppl type solution for the side on "square cylinder" will only exist if a curve can be identified, on which the two equations, that arise from setting the complex conjugate velocity at one of the symmetric vortices to be zero are satisified, provided that the vortices have a certain circulation. Such a solution has been identified (see figure 10) and a similar convergence of vortex cores is found as for the circular cross-section case. Curves have also been found for the corner on "square or triangular cylinders" and side on "triangular cylinders". It should be noted that there is not an analogue of the Föppl curve for all shapes, in particular the flat plate broadside on to the flow does not yield one, see Smith and Clark [14].

The final type of problem considered in this section is for a TYPE 1 body, where the cross-sectional shape varies with x. This can be achieved by specifying a longitudinal variation of the body shape parameters μ and λ with x. For all x, $\lambda = 0.5$ and μ has the following variation with x

$$\begin{array}{lcll} \mu & = & \mu_1 & x < 5. \\ \mu & = & \mu_A + \mu_B x + \mu_C x^2 + \mu_D x^3 & 5. < x < 25. \\ \mu & = & \mu_2 & 25. < x \end{array} \tag{13}$$

where μ_A, μ_B, μ_C and μ_D are determined by forcing μ to be continuous and $d\mu/dx = 0$ at $x = 5.0$ and $x = 25.0$. Since μ is fixed for $x > 25.0$, this type of problem again allows an appropriate conical solution to be calculated on the afterbody where the body cross-sectional shape is fixed. Figure 11 shows the effect of moving from a circular cross-section to a "triangular" cross-section with corner onto the flow. Here $\mu_1 = 0.5, \mu_2 = 0.9, \theta_{2s}(1) = 29.79^o$ and $\alpha = 3.0 \tan 5^o$. The solution furthest downstream is at $x = 42.5$. There is a very close agreement between the solution predicted by the non-conical calculation and the appropriate conical solution.

3.2 NON-CONICAL AMPLIFICATION

Results are now given for the flow past a 5^o circular cone, where the starting solution at the nose is a first family solution with a small asymmetry in the separation positions, with $\alpha = 3.4 \tan 5^o$. The separation positions were changed downstream so that they become symmetric, via

$$\begin{array}{lcll} \theta_{2s}(2) & = & 3^0 & x > 0 \\ \theta_{2s}(1) & = & 0^0 & 3 > x \\ \theta_{2s}(1) & = & -(x-3)^o & 3 < x < 10 \\ \theta_{2s}(1) & = & 3^0 & x > 10 \end{array} \tag{14}$$

The sheet shape in successive cross-flow planes is shown in figure 12, along with the appropriate symmetric conical solution in the last cross-flow plane, where $x = 30.0$. It is clear that although the final plane shown is far downstream from the point at which the separation positions become symmetric, the solution is not symmetric. The starboard sheet has a higher vertical extent than the corresponding symmetric conical solution and the port sheet is closer to the body than the symmetric solution. In figure 13 the normal and side force coefficients are plotted against x. It can be seen that the normal force for large x is close to that of the corresponding symmetric conical solution, however the side force grows downstream instead of decreasing to zero as it would need to do to match to the conical solution. The side force to normal force ratio increases steadily with x, see figure 14. The total circulation of each of the starboard and port sheets diverges from the corresponding conical solution value, see figure 15. Thus it appears that the small asymmetry is amplified downstream. A similar effect was noticed by Fiddes [5] in a preliminary study of a non-conical line-vortex model. The "non-conical amplification" is a distinct mechanism from the development of asymmetry on the conical nose itself. Fiddes conjectures that it is an important mechanism in the generation of side force at incidences below that required for the onset of second family solutions at the apex, see Fiddes and Williams [17]. It is possible that the solution is converging towards a second-family conical solution on the afterbody as $x \to \infty$. If this were the case it is possible that the first family, symmetric, solution could be unstable and the second family, asymmetric solution stable.

3.3 ASYMMETRIC SOLUTIONS

Consider a body of TYPE 2, where $\nu_1 = 5^o, \nu_2 = 3^o, a = 3.0$ and $b = 18.0$. The separation positions are given by $\theta_{2s}(1) = 180 - \theta_{2s}(2) = 6.87^o$ and incidence $\alpha = 4.6 \tan 5^o$. The vortex sheet shapes in successive cross-flow planes are shown in figure 16. The appropriate conical solution is shown on the afterbody for comparison, in the final downstream plane where $x = 20.0$. The vertical extent of the port sheet is greater in the conical solution on the afterbody than the non-conical prediction. The starboard conical sheet is straighter than the non-conical prediction, which has developed a more pronounced point of inflexion. Points of inflexion, were a common feature of

the asymmetric calculations and are believed to correspond to the formation of new centres of rotation, a phenomenon which is observed experimentally. The vortex-sheet model does not adequately represent the roll up of the new centres of rotation, and the Newton scheme fails soon after the development of the inflexion. This is a result of the fact that the sheet is not being substantially stretched and will develop a singularity, which leads to the breakdown of the solution procedure, see Moore [15], whose work for a time evolving vortex-sheet is analogous to the non-conical evolution if time t is replaced by convective time x/U. In order to make further progress downstream a procedure similar to that used by Hoeijmakers [18] to model the roll up of the wake behind the trailing edge of a wing would be required. The longitudinal variation of the normal and side force coefficients is shown in figure 17. The side force coefficient predicted by the non-conical calculation initially converges towards the conical value, but then starts to decrease and diverge from it. The normal force is also quite different from the conical value, but is still varying quite rapidly. Since the downstream solution is clearly not conical, this difference is not surprising. Figure 18 shows the ratio of side to normal force, although the ratio is decreasing with x from above the appropriate conical value it is not clear that its value is converging to the conical value. In fact it seems likely that this would not occur, since if the solution could be continued the point of inflexion on the starboard sheet is likely to become more pronounced downstream and thus move further from the appropriate conical solution. Figure 19 shows the longitudinal variation of the total circulation for the port and starboard sheets.

No solutions are given for bodies of TYPE 3. It proved impossible to track any solutions onto the afterbody. In the enforced symmetry solutions it was found that the non-conical solution on the afterbody was closely related to the Föppl solution for an infinite cylinder. Föppl solutions are stable to symmetric disturbances and unstable to asymmetric disturbances. This instability may be a significant factor in the failure to converge asymmetric solutions onto the afterbody.

Finally consider a varying cross-sectional shape problem, the body reference length again increases linearly with x and has a slope of 5^o, but the cross-sectional shape varies with x. Then for all x $\lambda = 0.5$, and μ has the same variation with x as given in (13).

Solutions for two different cases are shown in figure 20. Firstly figure 20a shows the effect on the downstream development of a second family solution of moving from a "square" cross-section, placed side onto the flow, to a circular cross-section. Here $\mu_1 = 0.76$ and $\mu_2 = 0.5$, the separation positions are $\theta_{2s}(1) = 180 - \theta_{2s}(2) = 27.50^o$ and $\alpha = 5.4 \tan 5^o$ The solution furthest downstream is at $x = 25.5$. Figure 20b shows the effect of moving from a "square" cross-section, with corner onto the flow, to a circular cross-section for a second family solution. Here $\mu_1 = 0.77$ and $\mu_2 = 0.5$, the separation positions are $\theta_{2s}(1) = 180 - \theta_{2s}(2) = 5.72^o$ and $\alpha = 4.2 \tan 5^o$. The solution furthest downstream is at $x = 35.5$. A comparison between the non-conical prediction and the appropriate conical afterbody solution reveals very different solutions in the final downstream plane shown. For the side on case the starboard vortex sheet of the conical solution has a tightly wound core lying much further inboard than the non-conical solution. However the starboard sheet is trying to wind up, as indicated by the inclination of the cut, but it still has a long way to go. (Note that it has been found that for a line-vortex calculation a tenfold increase in x from the start of the conical afterbody may be required before the solution gets near to a conical solution). Attempts to move further downstream were not successful and it is believed that this is principally due to the points of inflexion which form in the sheet. These inflexions cannot be tracked downstream using the current approach. The conical port sheet also extends further inboard than the corresponding non-conical prediction. For the corner on case, although the general shape of the conical and non-conical solutions on the circular afterbody are similar, the vertical extent of the starboard sheet is much greater in the non-conical prediction. Figure 21 shows the variation with x of the normal and side force coefficients. The values predicted by the non-conical calculation on the afterbody and the appropriate conical solution are not in agreement especially in the case of the side force. This is not surprising given the differences in the vortex sheet shapes. Again the development of points of inflexion in the non-conical solution, indicates that new centres of rotation may be trying to develop.

4 CONCLUSIONS

A comprehensive study has been undertaken of the solutions of the vortex-sheet model for flows past slender bodies with a wide range of cross-sections, some of which are shown in this paper. Although the model has a number of limitations that restrict its quantitative capabilities, it has identified physical mechanisms that have a dominant role in determining the qualitative features of slender separated flows. These features have now been confirmed by more advanced and accurate methods which solve the Euler and Navier-Stokes equations, see for example Marconi [19]. The calculation of symmetric solutions downstream has been successful and has provided several interesting solutions, which have helped to check the non-conical method. For asymmetric flows, tracking of solutions was hampered by the breakdown of the solution procedure associated with the development of points of inflexion in the vortex sheet corresponding to the formation of new centres of rotation, a phenomenon which is observed experimentally. Finally, a

non-conical amplification mechanism was found, distinct from the mechanism responsible for second family solutions at the apex. This mechanism may account for the observation of highly asymmetric separations on the afterbody, even when the incidence is low enough for the flow to be nearly symmetric at the nose.

References

[1] Legendre R., " *Écoulement au voisinage de la pointe avante d'une aile à forte flèche*", Rech. Aéro., Nos 30,31,35, (1953) Also:Progress in Aerospace Sciences, Volume 7.

[2] Smith J.H.B., *"Improved calculations of leading-edge separation from slender delta wings"*, RAE Technical Report 66070 (ARC 27897), (1966) Also: Proc. Roy. Soc. Lond. A, 306, pp67-90, (1968).

[3] Fiddes S.P., *"Separated flow about cones at incidence - theory and experiment"*, RAE Technical Memoranda AERO 2055, (1985) Also: In "Studies in vortex dominated flows", Proceedings of a conference at NASA Langley, Springer Verlag, (1987).

[4] Smith J.H.B., *"A theory of the separated flow from the curved leading edge of a slender wing"* ARC Reports and Memoranda 3116, (1957).

[5] Fiddes S.P., RAE Unpublished, (1982).

[6] Clark R.W., *"Non-conical flow past wings with leading-edge vortex sheets"*,ARC Reports and Memoranda 3814, (1978).

[7] Ashley H. and Landahl M., *"Aerodynamics of wings and bodies"*, Dover Publications Edition, (1985).

[8] Smith J.H.B., *"Boundary conditions on a vortex sheet"*, RAE Technical Memorandum AERO 1368, (1971).

[9] Williams Ann L. *"The effect of body shape on the development of vortex asymmetry in the flow past slender bodies"*, Presented at the 17th Congress of ICAS in Stockholm, Student Section, Also: Bristol University, Aero. Eng. Dept. Report No. 413, (1990)

[10] Williams Ann L., *"Separated flow past smooth slender bodies"*, Ph.D. Thesis, University of Bristol, (1991).

[11] Jones I.P., *"Leading-edge vortex flows"*, Ph.D. Thesis, University of East Anglia, (1974), Also:RAE Technical Report 80039 (1980) and Computers and Fluids, 3, pp155-177 (1975).

[12] Barsby J.E, *"Separated flow past a slender delta wing at low incidence"*, Aeronautical Quaterly, 24,(2),pp120-128, (1973).

[13] Lamb Sir H., *"Hydrodynamics"*, Sixth Edition, Cambridge University Press (1932).

[14] Smith J.H.B. and Clark R.W., *"Non-existence of stationary vortices behind a two-dimensional normal plate"*, AIAA Journal, 13, pp1114-1115,(1975).

[15] Moore D.W.,*"The stability of an evolving two-dimensional vortex sheet"*, Mathematika, 23, pp35-44, (1976).

[16] Smith J.H.B. , *"Private Communication*, (1990).

[17] Williams Ann L. and Fiddes S.P. *"Separated flows past smooth slender bodies at incidence"*, Bristol University, Aero. Eng. Dept. Report No. 454, (1991)

[18] Hoeijmakers H.W.M., *"Computational aerodynamics of ordered vortex flows"* NLR TR 88088 U, Also: Ph.D. University of Delft, the netherlands (1989).

[19] Marconi F., *"Asymmetric separated flows about sharp cones in a supersonic stream"*, 11th International Conference on Numerical Methods in Fluid Dynamics, Williamsburg, VA (1988).

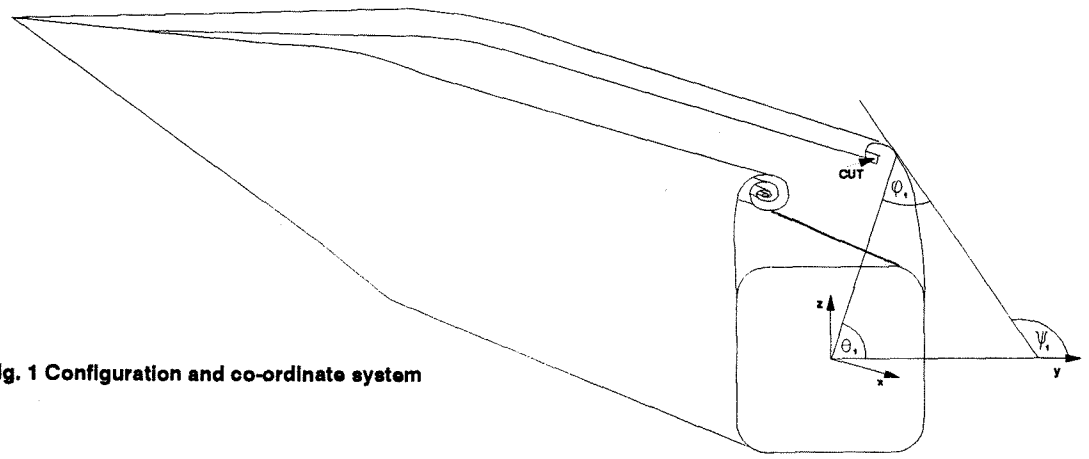

Fig. 1 Configuration and co-ordinate system

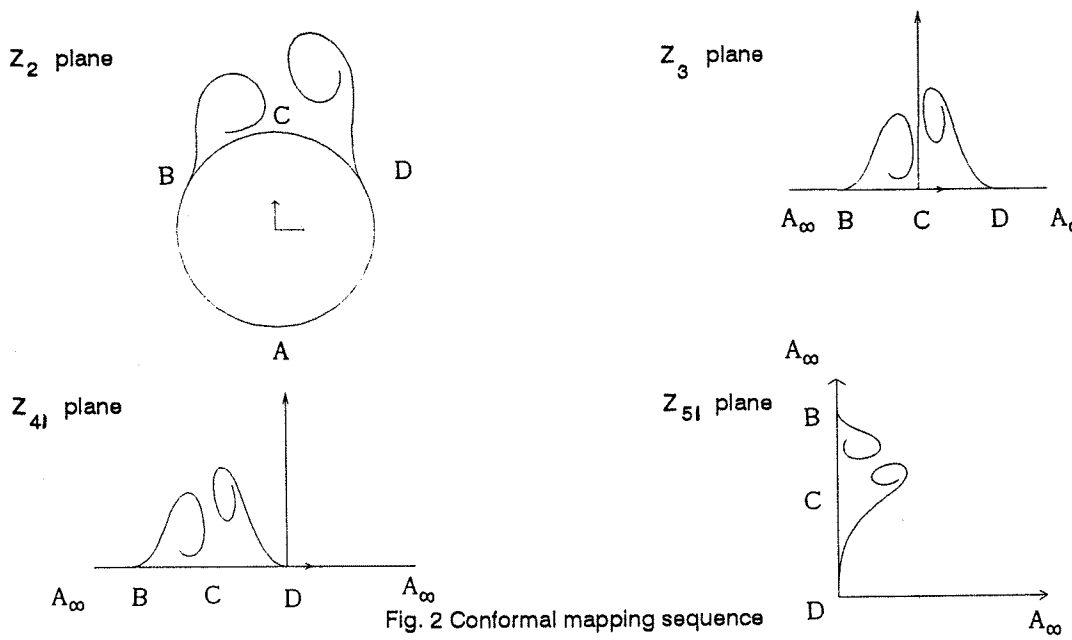

Fig. 2 Conformal mapping sequence

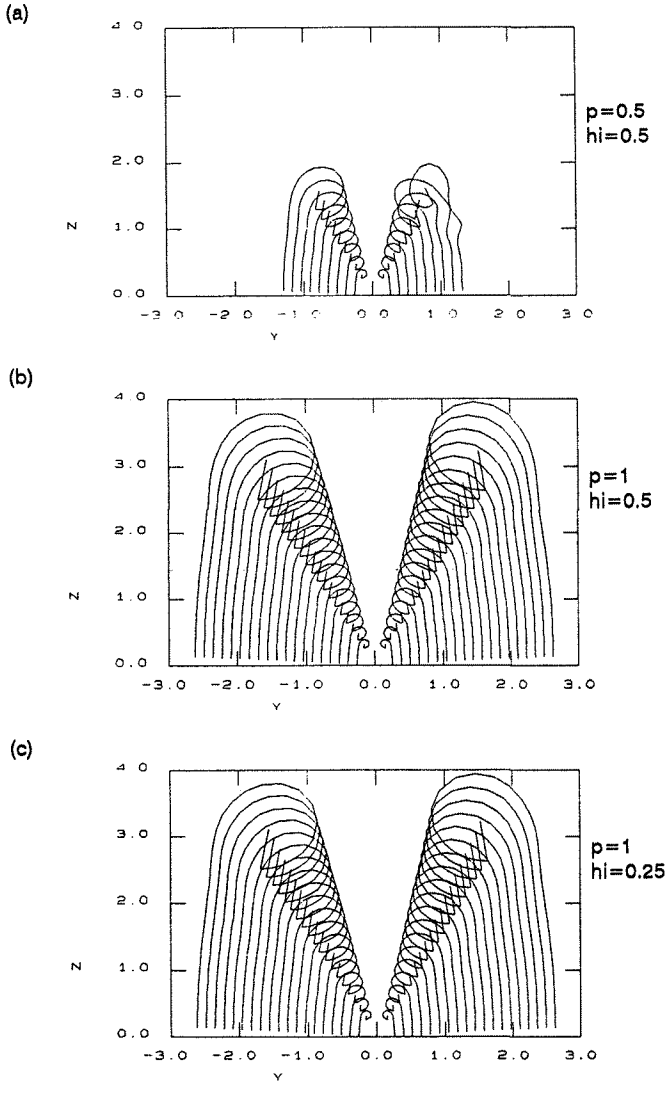

Fig. 3

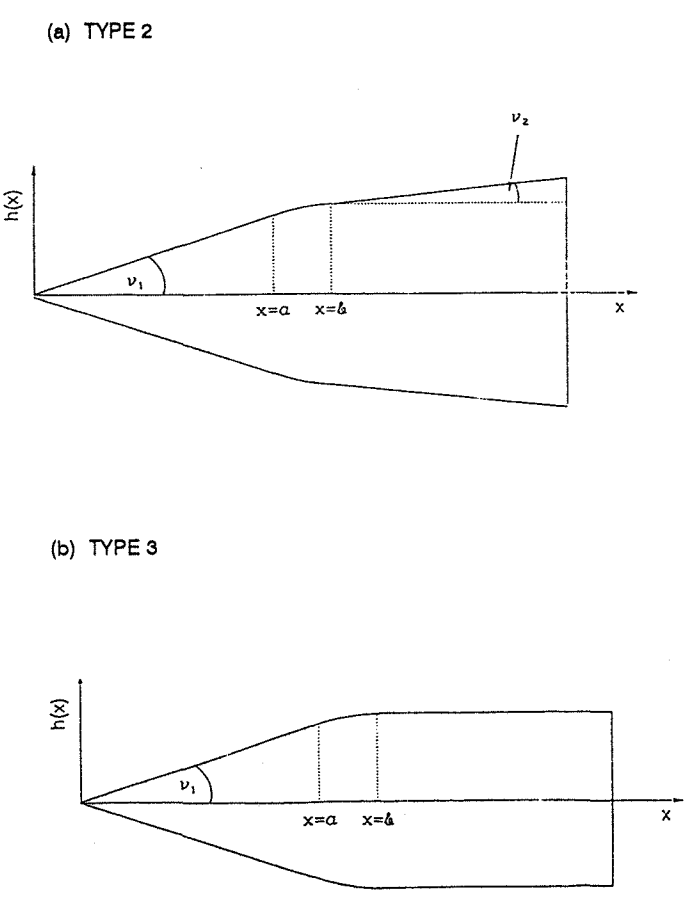

Fig. 4 Body shapes

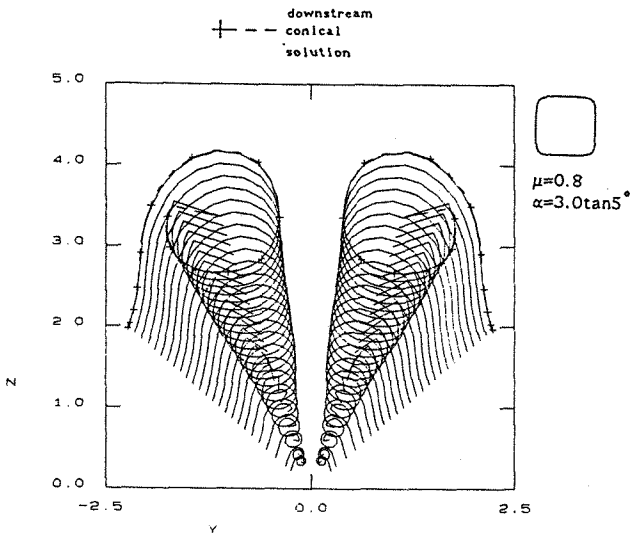

Fig. 5 "Square" cone/cone solution

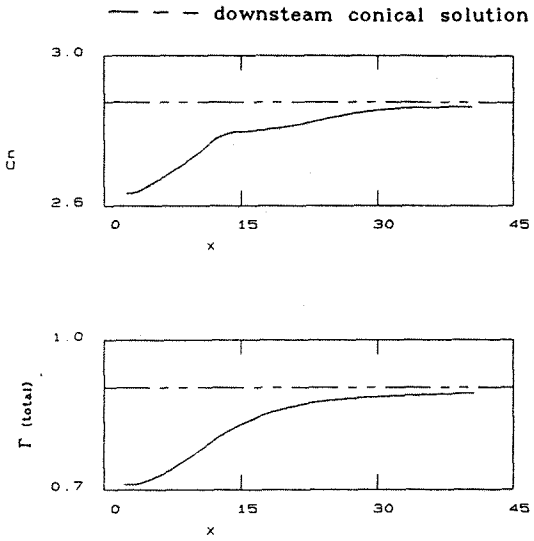

Fig. 6

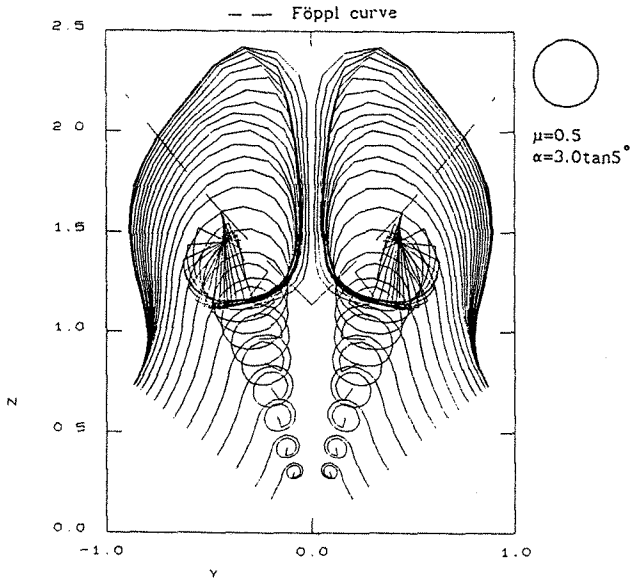

Fig. 7 Circular cone/cylinder solution

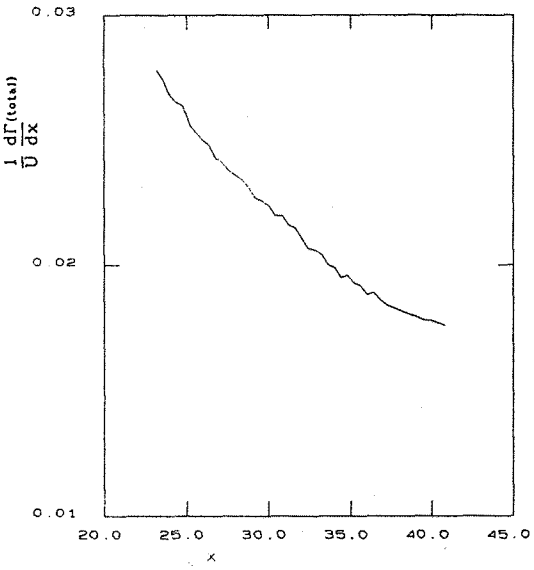

Fig. 8 Rate of change of total circulation with x

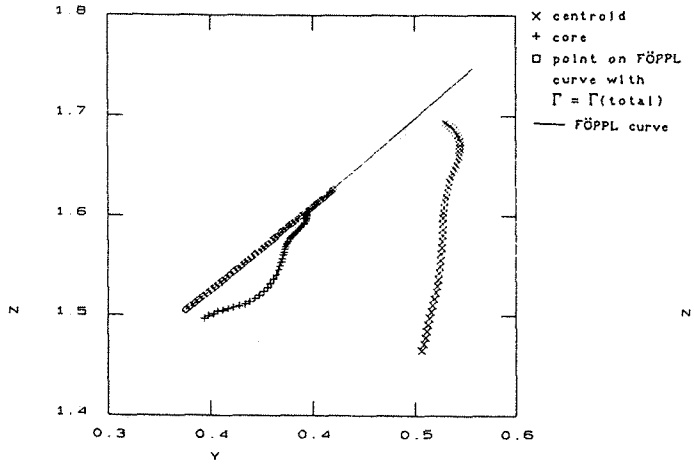

Fig. 9 Core and centroid positions compared with Foppl curve

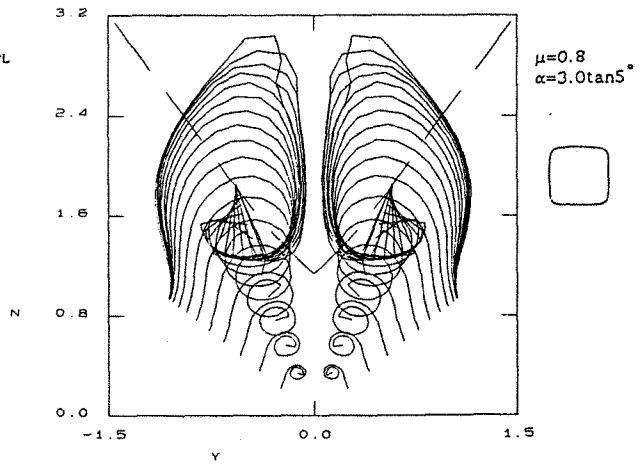

Fig. 10 "Square" cone/cylinder solution

— — — downstream conical solution

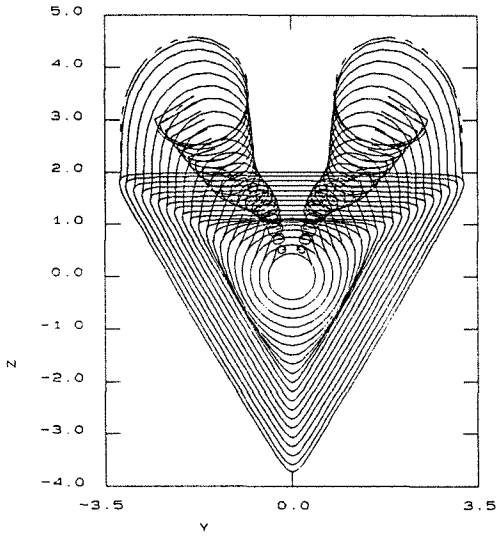

Fig. 11

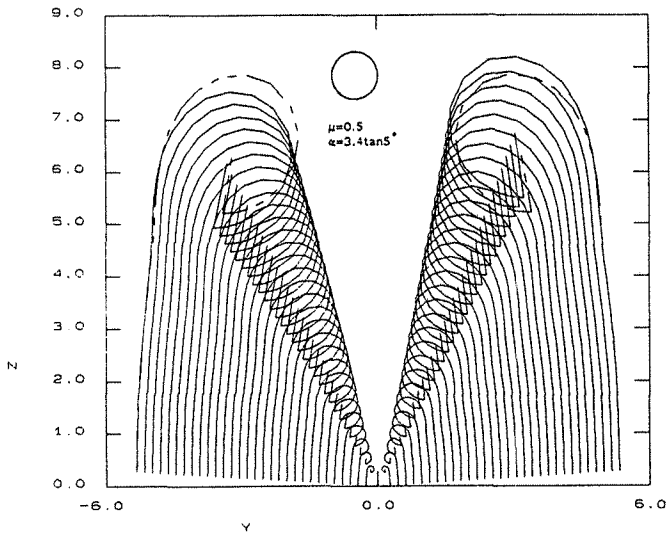

Fig. 12 Non-conical amplification of asymmetry

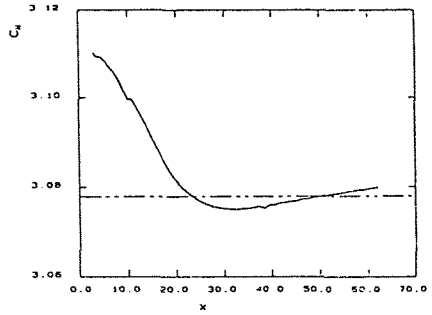

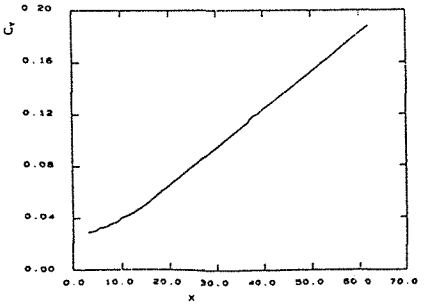

Fig. 13

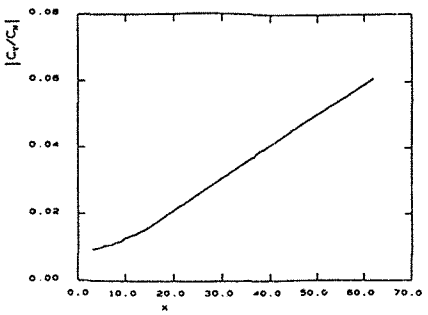

Fig. 14

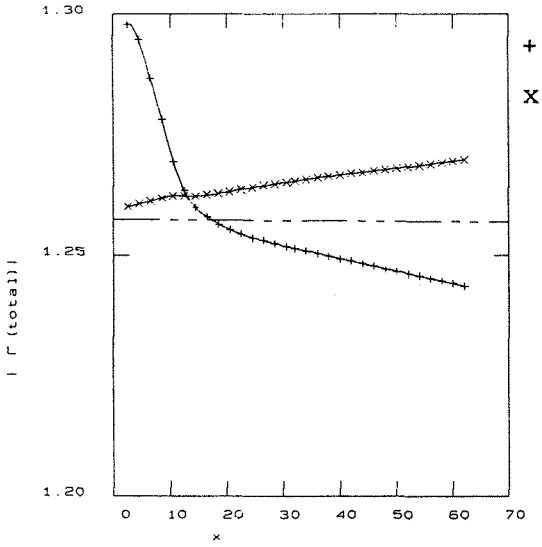

+ starboard

x port

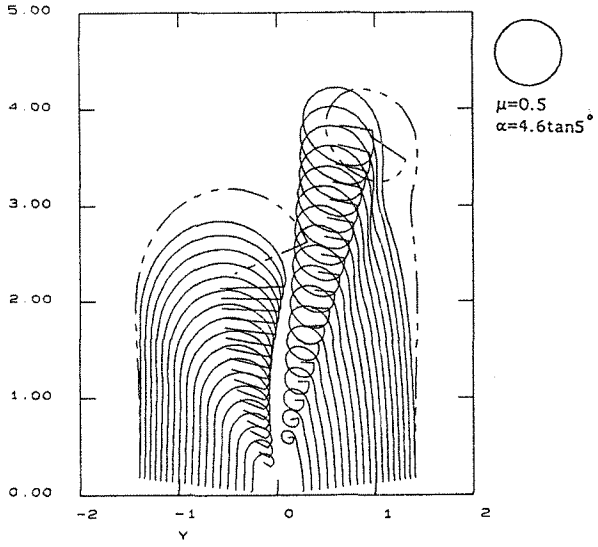

Fig. 15 Variation of total circulation with x

Fig. 16 Asymmetric cone/cone solution

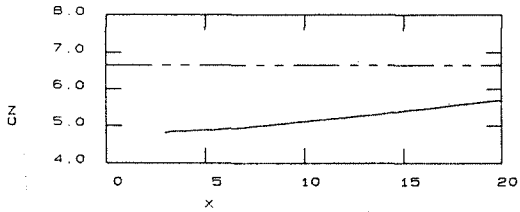

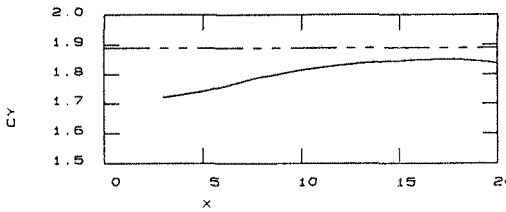

Fig. 17 Variation of normal and side force coefficients with x

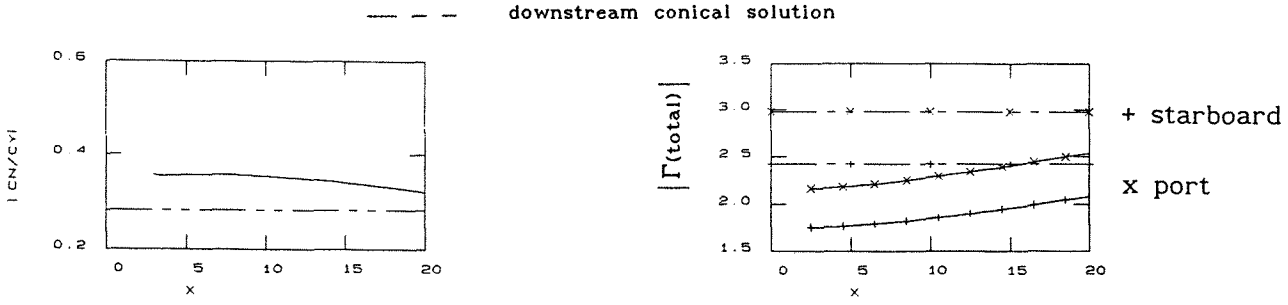

Fig. 18

Fig. 19

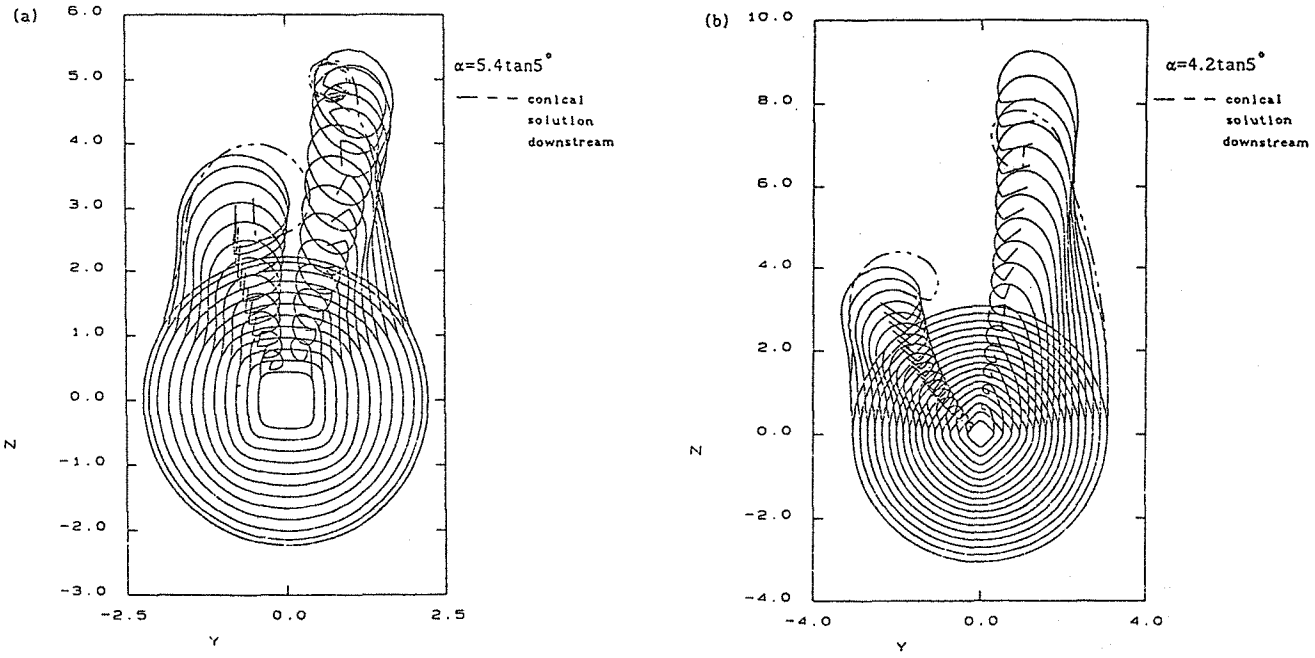

Fig. 20 Asymmetric solutions for bodies of varying cross-sectional shape

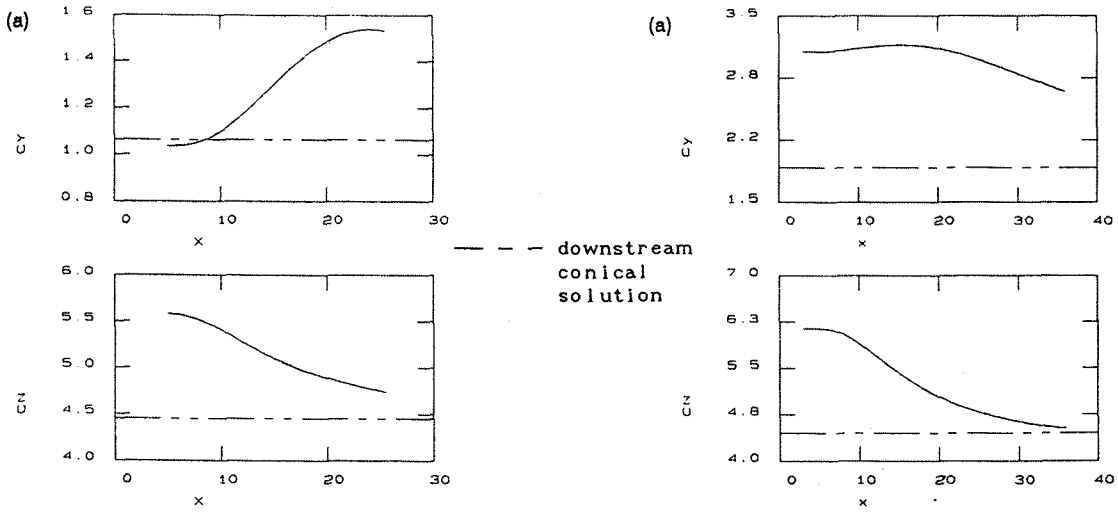

Fig. 21 Variation of normal and side force coefficients with x